

# Influence of interstitial Li on the electronic properties of $\text{Li}_x\text{CsPbI}_3$ for photovoltaic and battery applications

Wei Wei,<sup>1,2</sup> Julian Gebhardt,<sup>2</sup> Daniel F. Urban,<sup>2,3</sup> and Christian Elsässer<sup>1,2,3,\*</sup>

<sup>1</sup>*Freiburg Center for Interactive Materials and Bioinspired Technologies,  
University of Freiburg, Georges-Köhler-Allee 105, 79110 Freiburg, Germany*

<sup>2</sup>*Fraunhofer Institute for Mechanics of Materials IWM, Wöhlerstraße 11, 79108 Freiburg, Germany*

<sup>3</sup>*Freiburg Materials Research Center, University of Freiburg,  
Stefan-Meier-Straße 21, 79104 Freiburg, Germany*

(Dated: March 28, 2024)

The integrated device of a perovskite solar cell with a Li-ion battery is an innovative solution for decentralized energy storage in smart electronic devices. In this study, we examine the stability of Li ions intercalated in a  $\text{CsPbI}_3$  perovskite and their effect on the electronic structure of  $\text{Li}_x\text{CsPbI}_3$  compounds using first-principles density functional theory. Our simulations demonstrate that the insertion of Li at concentrations up to  $x = 1$  into  $\text{CsPbI}_3$  is energetically possible. Moreover, we identify that the distortion of the Pb-I octahedra has the strongest impact on the change in the electronic band gap. Specifically, an increase in the amount of intercalated Li causes larger structural distortions, which in turn lead to an increasing band gap as function of the Li content.

## I. INTRODUCTION

Advances in the design of smart electronic devices pose significant challenges for the integration and miniaturization of solar cells and energy storage components [1–4]. A promising approach involves the incorporation of halide perovskites as photovoltaic absorbers and Li-ion battery electrodes in commercial applications. Halide perovskites possess mixed ionic-covalent bonding character [5, 6], unlike the covalent or polar semiconductor compounds that are typically used in photovoltaic devices, and show good ionic conductivity [5]. Therefore, halide perovskite materials, which were originally designed for solar cells, may serve as multifunctional materials for both, light harvesting and Li storage.

The maximum amount of Li ions that can be stored in the unit cell of a perovskite crystal is determined by the quantity of available interstitial sites for the Li ions and their respective binding energies. Understanding and improving the performance of perovskite-based electrode materials for Li-ion batteries requires the knowledge of how the stability of materials is influenced by the intercalation of Li. Despite its importance, the interaction between inserted Li ions and the perovskite host crystal structure has not been studied extensively so far. Several experimental studies have looked at the structure and stability of Li-perovskite systems, and have reported a wide range of Li uptake limits of  $x = 0 - 6$  in  $\text{Li}_x\text{CsPbI}_3$  [7–10]. However, this wide range has not yet been comprehensively interpreted in the literature.

Furthermore, the insertion of interstitial elements always alters the electronic structure of the host crystal [11] which will have an influence on the performance of the solar cell [12]. While band gaps of Li-perovskite material systems have been measured experimentally [13, 14], the

relationship between the Li concentration and the band gap has not yet been systematically studied or explained.

In this work, we present a computational study based on density functional theory (DFT) to investigate the effects of Li-ion intercalation in  $\text{Li}_x\text{CsPbI}_3$  as a prototype.  $\text{CsPbI}_3$  is a well studied reference compound for inorganic halide-perovskite materials, with good light-harvesting capabilities [15–20]. We investigate two structural scenarios that serve as limiting cases for the dynamic  $\text{CsPbI}_3$  perovskite structure under device-operation conditions [21]. The two cases, namely the cubic  $\alpha$  structure and the distorted  $\gamma'$  structure, represent the highest saddle point configuration and the configurations at the local energy minima (when tetragonal lattice distortions are neglected) of the vibrating  $\text{CsPbI}_3$  crystal, respectively. We study the Li uptake limit in the  $\text{CsPbI}_3$  perovskite structure for both cases, and the influences of Li on the crystal and electronic structures of  $\text{CsPbI}_3$  are systematically explored.

The paper is organized as follows. Section II introduces the computational setup and the definition of the formation energy of Li inserted into  $\text{CsPbI}_3$ . In Sec. III, we present the results on the stability of interstitial Li within  $\text{CsPbI}_3$  and its influence on the electronic structure. In Sec. IV, we discuss our results in view of other findings in the literature, and we summarize and conclude in Sec. V.

## II. COMPUTATIONAL DETAILS

All calculations are carried out with the Vienna ab initio simulation package (VASP) [22] employing projector-augmented waves [23] and the semi-local Perdew-Burke-Ernzerhof (PBE) [24] exchange-correlation functional. An energy cutoff of 520 eV was used for the plane-waves basis. Total-energy differences and forces on atoms for all structural degrees of freedom are converged within

---

\* christian.elsaesser@iwmm.fraunhofer.de

$1 \times 10^{-5}$  eV and  $5 \times 10^{-3}$  eV/Å, respectively. The Brillouin-zone integrals were sampled by  $4 \times 4 \times 4$  Monkhorst-Pack  $k$ -point grids [25] with a Gaussian smearing of  $1 \times 10^{-3}$  eV for the  $2 \times 2 \times 2$  supercell models, containing 40 atoms (i.e., eight  $ABX_3$  formula units). Structural relaxations for these systems are carried out in internal coordinates [26]. The implementation was improved to retain the initially set symmetry of the crystal.

To obtain an accurate lattice constant, we used the Tkatchenko-Scheffler (TS) correction [27] for the calculations of the cubic  $\alpha$  structure. The obtained equilibrium lattice constant is  $a_0(\text{PBE}+\text{TS})=6.17$  Å, which is in good agreement with the experimental value of  $a_0(\text{Expt.})=6.18$  Å [28]. For the  $\gamma'$  structure we used the PBE exchange-correlation functional without TS correction and obtained an equilibrium lattice constant  $a_0(\text{PBE})=6.32$  Å.

The defect formation energies of Li ions intercalated at interstitial sites in the perovskite crystal are calculated as

$$E_{\text{form}} = \frac{E_{\text{tot}}[\text{Li}_x\text{CsPbI}_3] - E_{\text{tot}}[\text{CsPbI}_3] - x_{\text{Li}}E_{\text{tot}}[\text{Li}_{\text{bcc}}]}{x_{\text{Li}}}, \quad (1)$$

where  $E_{\text{tot}}[\text{Li}_x\text{CsPbI}_3]$  is the total energy of the considered perovskite crystal containing Li,  $E_{\text{tot}}[\text{CsPbI}_3]$  is the energy of the reference crystal without Li,  $E_{\text{tot}}[\text{Li}_{\text{bcc}}]$  is the energy per Li atom in the body-centered cubic one-atom unit cell of the elemental Li metal, and  $x_{\text{Li}}$  is the proportion of Li per formula unit of the perovskite crystal. The calculated lattice constant of the body-centered cubic Li metal is 3.42 Å, and the total energy of metallic Li was computed using a  $10 \times 10 \times 10$  Monkhorst-Pack  $k$ -point grid (and otherwise identical technical parameters).

For calculating the electronic structure, we employ the DFT+1/2 method [29] including spin-orbit coupling [30]. This methodology provides an accurate electronic-structure description for  $\text{CsPbI}_3$  perovskites, as demonstrated in our previous study [31].

### III. RESULTS

#### A. The stability of interstitial Li in $\text{CsPbI}_3$

We studied two structural models, the  $\alpha$  and  $\gamma'$  structures, to represent the two limiting cases of the dynamical  $\text{CsPbI}_3$  phase at finite temperature. Figure 1 illustrates these two models. The ordered cubic  $\alpha$  structure is observed as a temporal and spatial average in experimental studies [32, 33] and represents the highest saddle-point energy configuration of the phase, while the disordered  $\gamma'$  structure is obtained as the configuration of the local energy minimum of the  $\alpha$  phase. Note that in reality the tetragonal lattice distortions towards the  $\gamma$  phase, which are observed at lower temperatures, are likely to occur in an averaged manner at higher temperatures, too. However, the influence of the concomitant small structural

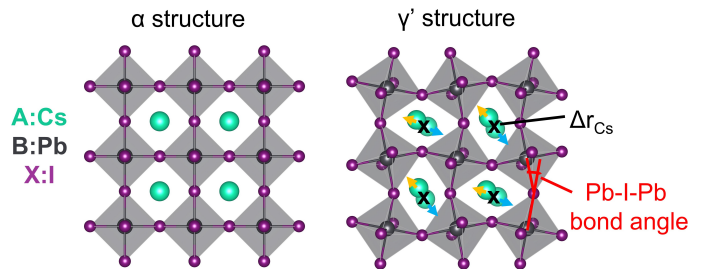


FIG. 1: The two limiting models of the dynamic crystal structure of  $\text{CsPbI}_3$ , illustrating the degrees of structural distortion. The B-site atoms are located on the lattice points of the cubic (pseudo-cubic) structure. The off-center displacement of the A-site atoms ( $\Delta r_{\text{Cs}}$ ) and the tilts of B-X octahedra described by the averaged Pb-I-Pb bond angle difference ( $\Delta_{\text{Pb-I-Pb}}$ ) quantify the structural distortion.

changes is weak, [21, 34] (e.g., the  $\gamma$  phase is more stable than the  $\gamma'$  structure by only 4.2 meV per unit cell) and, therefore, neglected for the remainder of this study. The structural difference between  $\alpha$  and  $\gamma'$  can be attributed to two factors: the off-center displacement of the A-site Cs atoms ( $\Delta r_{\text{Cs}}$ ), and the octahedral B-X tilts that occur around two axes [35] in the  $ABX_3$  compound  $\text{CsPbI}_3$ . Here, we quantify these octahedral tilts by the averaged Pb-I-Pb bond angle difference ( $\Delta_{\text{Pb-I-Pb}}$ ).

In the following, we study the stability of interstitial Li as function of its concentration in the two structural models using a  $2 \times 2 \times 2$  supercell. By subsequently adding Li to the two models,  $\text{Li}_x\text{CsPbI}_3$  was obtained with Li concentrations varying from  $x=1/8$  to  $x=1$  for the  $\alpha$  structure, and  $x=1/8$  to  $x=2$  for the  $\gamma'$  structure. We analysed various different Li arrangements in the two models, as Li-Li interactions need to be considered for Li concentrations above the dilute limit.

##### 1. The stability of interstitial Li in the $\alpha$ structure

In the  $\alpha$  structure, the high-symmetry interstitial sites are three octahedral (O) and eight tetrahedral (T) sites as displayed in Fig. 2a. The O site is located in the center of an octahedron formed by two Cs atoms and four I atoms, while the T site is located in the center of a tetrahedron formed by one Cs atom and three I atoms.

Figure 2b shows the formation energies of Li in both interstitial sites ranging from 0.16 to 1.65 eV for  $x=1/8$  to  $x=1$ . We study the influence of varying the Li concentration  $x$  by: i) excluding changes to the lattice constant ( $V_{\text{fixed}}$ ), ii) optimizing the volume ( $V_{\text{opt}}$ ), and iii) allowing full relaxation of unit-cell degrees of freedom ( $E_{\text{opt}}$ ) for each  $x$ . The highest point symmetry of a Li atom on an O site ( $D_{4h}$ ) or a T site ( $C_{3v}$ ) is maintained at every concentration  $x$  in all three cases.

For the fixed cell at low concentrations of  $x=1/8$  and  $x=1/4$ , the insertion of Li atoms at the O sites is energetically

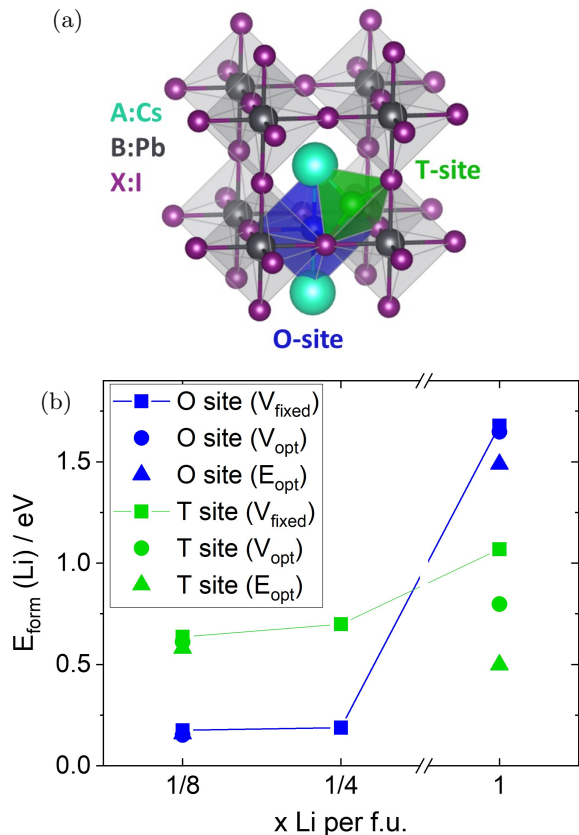


FIG. 2: a) Li interstitial sites in the  $\alpha$  structure, located in the center of an octahedron (O) or a tetrahedron (T) formed by host lattice atoms. b) Formation energies of interstitial Li as function of the concentration  $x$ . Square symbols indicate results obtained for a fixed simulation cell ( $V_{\text{fixed}}$ ), circle symbols indicate that the volume of the cell was optimized, but the rectangular shape of the cell was maintained during optimization ( $V_{\text{opt}}$ ), and the triangle symbols indicate structural relaxation in all degrees of freedom ( $E_{\text{opt}}$ ). The point symmetry of the interstitial Li at the O site ( $D_{4h}$ ) or T site ( $C_{3v}$ ) is maintained for all Li concentrations.

ically more favorable by approx. 0.4 eV compared to the T sites. At  $x=1/8$ , the  $E_{\text{form}}$  on the O site is 0.18 eV, and an optimization of lattice degrees of freedom does not further stabilize the interstitial site. Increasing the concentration to  $x=1/4$  gives a similar  $E_{\text{form}}$  of 0.19 eV for the O site. In contrast, the results for  $x=1$  differ significantly from those for the two lower concentrations. The order of  $E_{\text{form}}$  of the two sites is reversed and, compared to  $x=1/4$ , the formation energy of Li is increased by at least 0.37 eV (when changes in lattice parameters are excluded). This is due to Li-Li interactions in these structures. Allowing the volume to adjust to the Li content ( $V_{\text{opt}}$ ), a stabilization of 0.03 eV (0.27 eV) is found accompanied by an increase of the volume by 4% (14%) with Li on the O (T) sites. Further structural distortions away from the cubic structure, by relaxing all lattice pa-

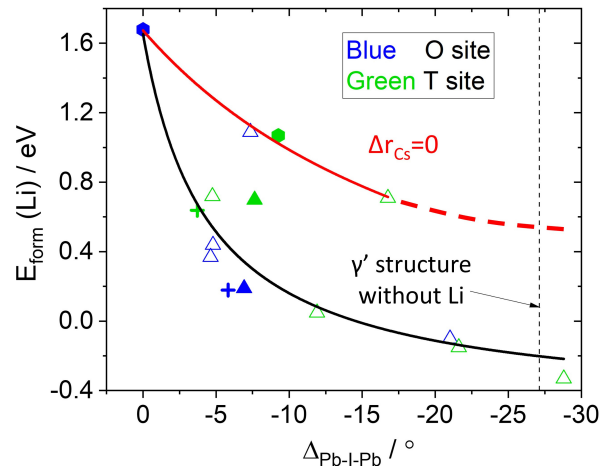


FIG. 3: The relationship between the formation energy of interstitial Li and the structural distortion  $\Delta_{\text{Pb-I-Pb}}$  with varying Li concentration  $x$  in the  $\alpha$  structure at fixed volume and cell shape. Blue and green symbols indicate interstitial Li on O and T sites, respectively. Different concentrations are indicated as  $x=1/8$  (+),  $x=1/4$  ( $\Delta$ ), and  $x=1$  ( $\square$ ). Filled and open symbols represent high and low-symmetry structures of the  $\text{Li}_x\text{CsPbI}_3$  compounds, respectively. Higher energy structures, fitted by the red curve, are structures where  $\Delta r_{\text{Cs}}=0$ , due to symmetry constraints in the  $\alpha$  structure. In the lower energy structures, fitted by the black curve, a pronounced Cs off-center displacement is accompanying the angle distortion.

rameters ( $E_{\text{opt}}$ ), are energetically stabilized by 0.19 eV (0.58 eV). The lattice undergoes a tetragonal distortion with the insertion of Li at the O site, while the insertion of Li at the T site transforms the lattice into a rhombohedral cell with a cell-edge angle of  $79^\circ$ .

In order to study the relevance of Li-Li interactions we investigated a variety of Li arrangements for  $x=1/4$ . We have not computationally enforced the high symmetry during the structural relaxations that we carried out at fixed lattice parameters. The considered arrangements of Li atoms may affect their energetics in the perovskite crystal due to different Li-Li distances. We do not find a clear relationship between the Li-Li distances and the formation energy. Instead, we observe that the formation energy is associated with structural distortions of the host lattice, shown in Figure 3, as quantified by  $\Delta_{\text{Pb-I-Pb}}$  and  $\Delta r_{\text{Cs}}$ . This observation holds true for all concentrations and Li arrangements investigated for the  $\alpha$  structure. The formation energy decreases with increasing  $\Delta_{\text{Pb-I-Pb}}$ . This trend can be effectively described by an exponential relationship ( $y = a \cdot e^{\frac{b}{x+c}} + d$ ), as depicted by the black line in Figure 3, with  $x = \Delta_{\text{Pb-I-Pb}}$  and  $y = E_{\text{form}}$ . There are exceptions with significantly higher formation energies in cases where the second measure of host lattice distortion,  $\Delta r_{\text{Cs}}$ , is equal to zero. Another exponential fitting curve describes these exceptions, as il-

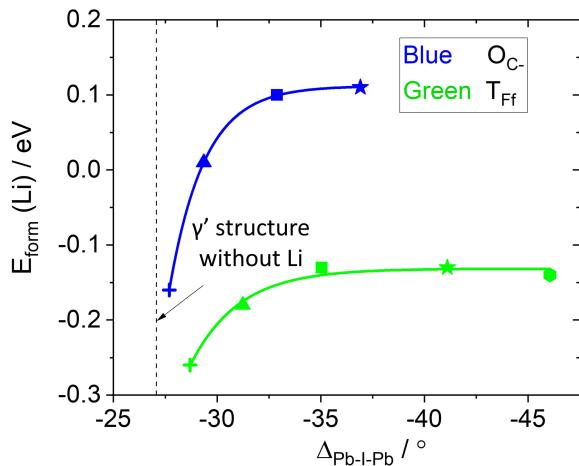


FIG. 4: The relationship between the formation energy of interstitial Li and the structural distortion  $\Delta_{\text{Pb-I-Pb}}$  for the most stable O and T sites with varying Li concentration  $x$  in the  $\gamma'$  structure. Different concentrations are indicated as  $x=0$  ( $\bullet$ ),  $x=1/8$  ( $+$ ),  $x=1/4$  ( $\Delta$ ),  $x=1/2$  ( $\square$ ),  $x=3/4$  ( $\star$ ),  $x=1$  ( $\circ$ ).

illustrated by the red line. The cases where  $\Delta r_{\text{Cs}} \neq 0$  have lower formation energies than the case where  $\Delta r_{\text{Cs}} = 0$ . As the two structural distortions increase, the  $\alpha$  structure transforms to the  $\gamma'$  structure, accompanied by a decrease in the formation energy.

Therefore, the stability limit for interstitial Li in  $\text{CsPbI}_3$  while maintaining the symmetry of the  $\alpha$  structure is at  $x=1/4$ . For structures with  $x=1/2$  it is impossible to maintain this high symmetry with a reasonable Li distribution.

## 2. The stability of interstitial Li in the $\gamma'$ structure

Due to the lower symmetry of the  $\gamma'$  structure compared to the  $\alpha$  structure, the six O and eight T interstitial sites are no longer symmetry equivalent. After optimization, the most stable T and O sites have formation energies of -0.26 and -0.16 eV per Li atom, respectively, in the 40-atoms supercell, i.e. at a Li concentration of  $x=1/8$ . We label these two most stable interstitial sites as  $\text{T}_{\text{FF}}$  and  $\text{O}_{\text{C-}}$  in accordance with the nomenclature introduced in our preceding work [21].

Figure 4 summarizes the Li formation energy of interstitial Li in the  $\gamma'$  structure for  $x=0, 1/8, 1/4, 1/2, 3/4$ , and 1, on the  $\text{T}_{\text{FF}}$  and  $\text{O}_{\text{C-}}$  sites. In this model, the Li atoms are arranged as far away from each other as possible in the given supercell. Higher concentrations of Li consistently result in stronger structural distortions, but do not always lead to higher formation energies. From  $x=1/8$  to  $x=1/2$ , the formation energy increases with increasing structural distortion  $\Delta_{\text{Pb-I-Pb}}$ . When  $x$  exceeds  $1/2$ ,  $E_{\text{form}}$  reaches a plateau. By further increasing  $x$  to 1 on  $\text{T}_{\text{FF}}$  sites, a slight decrease of  $E_{\text{form}}$  is observed.

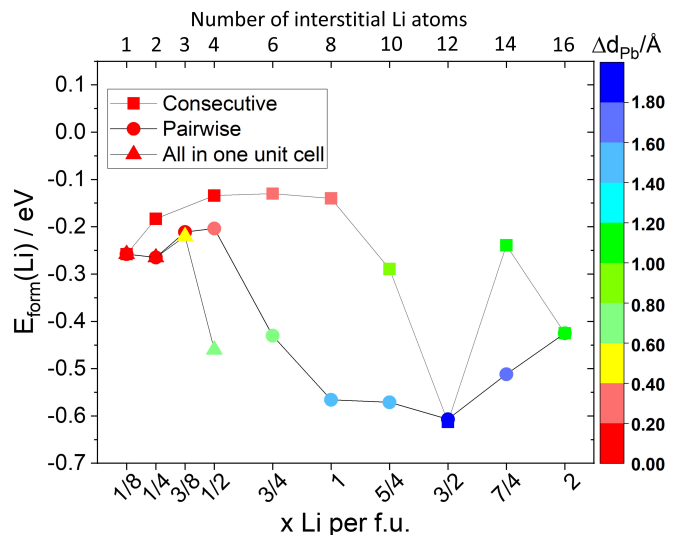


FIG. 5: Formation energies of Li intercalation in the  $\gamma'$  structure with different Li concentrations up to  $x=2$ . The symbols denote consecutive ( $\square$ ), pairwise ( $\circ$ ) and all in one f.u. ( $\Delta$ ) distributions of Li atoms, respectively. The distortion beyond the pseudo-cubic structure is evaluated by the average displacement of the B-site Pb atoms ( $\Delta d_{\text{Pb}}$ ), for which the magnitude is illustrated by the color code.

However, Li is no longer stable on  $\text{O}_{\text{C-}}$  sites in structures with  $x=1$  and the Li atoms move to the neighboring  $\text{T}_{\text{FF}}$  sites during the geometry optimization. The energy profile is again consistent with the  $\gamma'$  structure being the energetically most favorable structure. An increase in Li content leads to an increased structural deformation and an increase in energy. The minimum energy is obtained for a Li content of  $x = 1/8$  for which the resulting crystal structure is closest to the  $\gamma'$  structure.

According to the result that the interstitial Li does not further destabilize the perovskite structure by increasing the Li concentration beyond  $x \geq 1/2$ , we suggest that even concentrations of  $x > 1$  may be energetically accessible for Li insertion into the  $\gamma'$  structure. Therefore, we also investigate several hypothetical but plausible arrangements for Li concentrations up to  $x=2$  at the  $\text{T}_{\text{FF}}$  sites in the  $\gamma'$  structure (allowing all structural degrees of freedom to change).

To explore viable options for incorporating Li atoms into the perovskite structure, we evaluate three potential strategies for constructing structures with increasing Li concentration: i) by consecutively adding one Li to each empty  $\text{ABX}_3$  unit cell until  $x=1$ , cf. Fig. 4, then adding the second Li to each unit cell in the same order until  $x=2$ ; ii) by pairwise adding two Li atoms to each empty unit cell in the supercell; and iii) by adding all Li atoms to the same unit cell (up to  $x = 1/2$ ). These strategies explore the stability of interstitial Li atoms from the most uniform to the most clustered Li distributions.

As  $x$  increases, we quantify the structural distortion of

the perovskite structure by the average displacement of the B-site atoms ( $\Delta d_{\text{Pb}}$ ), and indicate the distortion by a color code in Fig. 5. This displacement of Pb atoms affects the bonding within the  $\text{PbI}_6$  octahedra, resulting in a strong structural deformation away from the cubic or pseudo-cubic structures of our perovskite models. More specifically, when  $\Delta d_{\text{Pb}} > 0.4 \text{ \AA}$  (as indicated by the yellow color in the figure), the octahedra start to deform significantly.

We emphasize here that identifying the correct structural model is difficult in computational studies because the structures obtained by atomic relaxation are inherently constrained by the symmetry and unit cell of the chosen starting structure. Nevertheless, since the observed deformations in our model structures are energetically favored, this indicates that phases with such high Li concentrations can form. However, the potential irreversibility of such structural changes upon subsequent Li removal needs to be investigated further.

In summary, we find that the Li uptake limit of the  $\gamma'$  structure of  $\text{CsPbI}_3$  is  $x=1$ . Concentrations of  $x > 1$  always lead to severe and potentially irreversible structural changes (with Pb shifts of  $\Delta d_{\text{Pb}} > 0.4$ ).

## B. Electronic structure analysis

In the following we investigate the effect of interstitial Li atoms on the electronic band gap of the  $\text{CsPbI}_3$  perovskite. We examine several factors, such as the Li-induced structural distortion, the electronic screening, and the defect states in the band gap related to the interstitial Li atoms. We limit the examined Li concentrations to  $x \leq 1$  due to the instability of the perovskite structure for higher Li concentrations.

The relationship between the band gap  $E_g$  and the variation of the bond angle  $\Delta_{\text{Pb-I-Pb}}$  for the  $\alpha$  and  $\gamma'$  structures is illustrated in Fig. 6 (a). We find a relationship between the two variables that appears linear across the high and low symmetry arrangements of Li in structures that were derived by adding Li into the  $\alpha$  structure (red symbols). The structure with  $x=1$  for the insertion of Li at the O site is an outlier, as it maintains the host crystal structure due to an artificially high symmetry. The band gap increases as the Li concentration rises. This growth trend is consistent with the earlier analysis of the structural distortion that arises when the Li content increases, i.e., increasing  $x$  leads to an increase of  $\Delta_{\text{Pb-I-Pb}}$ , which in turn increases  $E_g$ .

In the  $\gamma'$  structure, we observe a similar linear relationship between  $E_g$  and  $\Delta_{\text{Pb-I-Pb}}$  (black symbols). However, the two linear regimes differ in slope and axis intercept.

The strong dependence of  $E_g$  on  $\Delta_{\text{Pb-I-Pb}}$ , which is in line with the different band gaps of the  $\alpha$  structure (1.01 eV,  $\Delta_{\text{Pb-I-Pb}}=0^\circ$ ) and the  $\gamma'$  structure (1.88 eV,  $\Delta_{\text{Pb-I-Pb}}=-27^\circ$ ), indicates that the structural changes dominate the influence that interstitial Li atoms have on the electronic structure of  $\text{CsPbI}_3$ . This is in line with

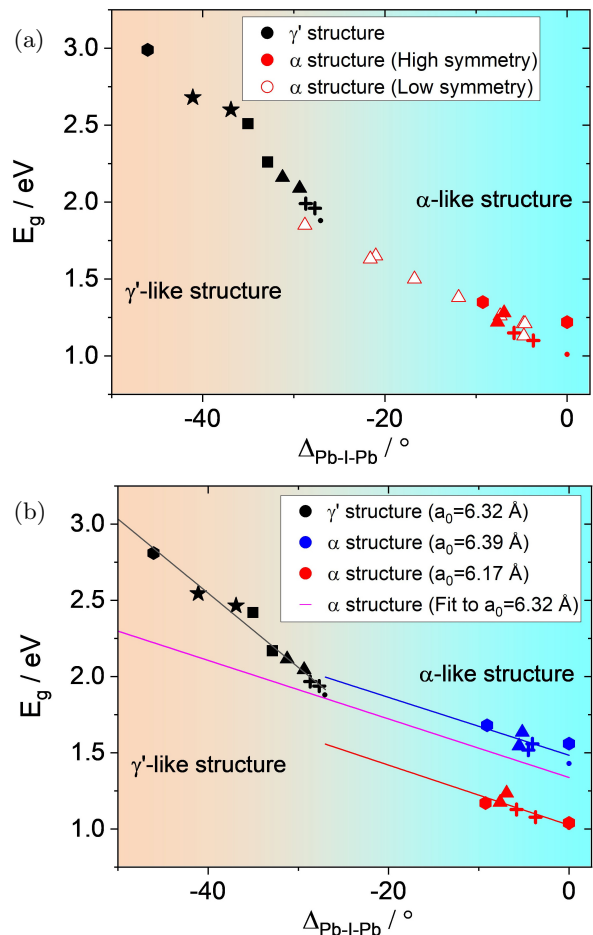


FIG. 6: (a) Band gap  $E_g$  vs.  $\Delta_{\text{Pb-I-Pb}}$  for  $\text{Li}_x \text{CsPbI}_3$  with different Li content  $x$  and Li distribution. Black and red symbols denote Li in the  $\gamma'$  and  $\alpha$  structures, respectively. Orange and light blue colored areas indicate the structural regimes, respectively. Different concentrations are indicated as  $x=0$  ( $\bullet$ ),  $x=1/8$  ( $+$ ),  $x=1/4$  ( $\triangle$ ),  $x=1/2$  ( $\square$ ),  $x=3/4$  ( $\star$ ),  $x=1$  ( $\circ$ ). Filled symbols refer to structures that retain  $D_{4h}$  and  $C_{3v}$  symmetry for O and T sites in the  $\alpha$  structure, respectively. Other lower symmetry arrangements of Li are indicated by open symbols. (b) Band gaps obtained after subtracting the influence of  $x$  extra electrons in the conduction band, estimated as  $x \cdot 0.18 \text{ eV}$  (see text for details). Two volumes are compared for the  $\alpha$  type structures. The resulting averaged trend for the volume of the  $\gamma'$  structure is shown as magenta line.

the notorious sensitivity of band gaps in group-IV halide perovskite structures to the octahedral tilt angles [36].

To understand the direct effects of the insertion of Li atoms on the electronic structure of a  $\text{CsPbI}_3$  crystal, we analyze the density of states (DOS) in the proximity of the band gap in Fig. 7a. Upon the addition of Li to the  $\alpha$  structure, the Fermi level ( $E_F$ ) shifts to the edge of the conduction band for  $x > 0$ . An interstitial Li atom adds

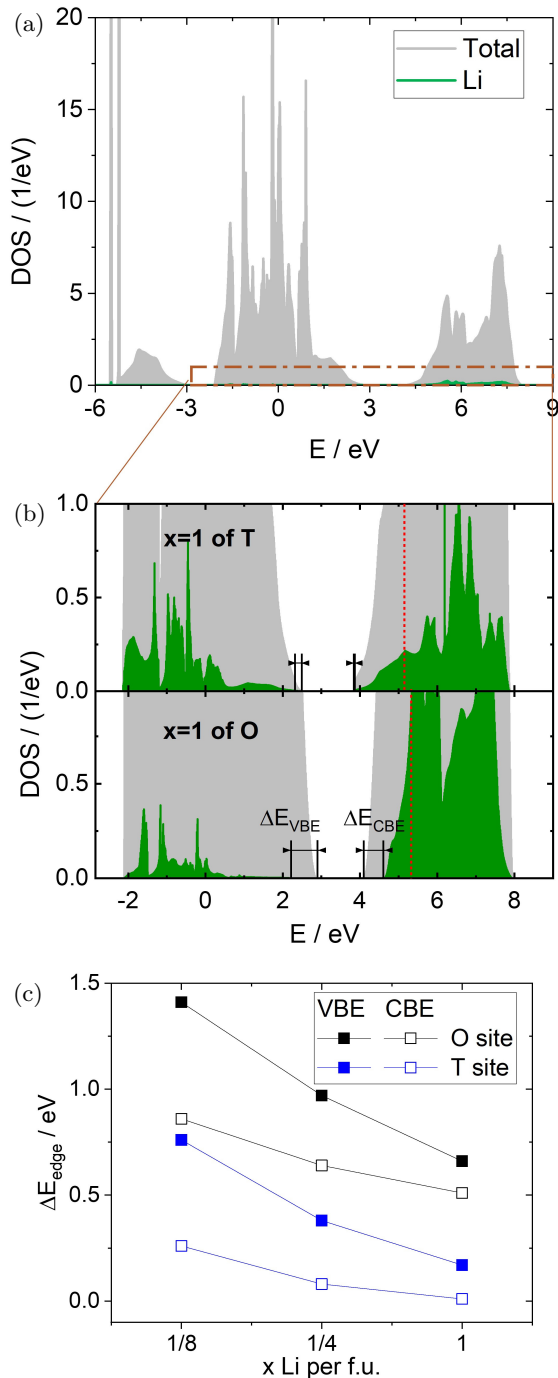


FIG. 7: (a) DOS of  $\text{Li}_x\text{CsPbI}_3$  in the  $\alpha$  structure and (b) the detailed DOS for interstitial Li on the O and T site with  $x=1$ . Structures with  $D_{4h}$  and  $C_{3v}$  symmetry are considered for O and T sites, respectively. Total DOS (gray) and Li projected DOS (green) are shown.  $E_F$  is indicated by red dashed lines and the energy separation of bands containing Li contributions from the two band edges,  $\Delta E_{VBE}$  and  $\Delta E_{CBE}$ , are marked by black lines and labels (c) The energy separation of bands with Li content from either band edge,  $\Delta E_{edge}$  (edge: VBE or CBE), for  $\text{Li}_x\text{CsPbI}_3$  with varying  $x$  in the  $\alpha$  structure.

its  $1s$  orbital as a deep core state (not shown). The  $\text{Li } 2s$  orbital remains mostly unoccupied, but hybridizes with Pb and I orbitals in the regions of the conduction and valence band edges (CBE and VBE), respectively. For small concentration  $x$  of Li, there is a significant distance of states with Li contributions to the two band edges ( $\Delta E_{VBE}$  and  $\Delta E_{CBE}$ , see Fig. 7b). With increasing  $x$  of Li, this distance shrinks (see Fig. 7c). This implies that Li affects the local environment of more I and Pb atoms as the value of  $x$  increases. When Li atoms are located on the T sites, their contribution to the DOS has a broader distribution in energy, compared to Li atoms at the O sites at the same concentration. This indicates a stronger hybridization of Li with the Pb and I orbitals on the T sites than on the O sites.

We have also analyzed the DOS for various concentrations of interstitial Li in the  $\gamma'$  structure and obtain qualitative similarities to the findings for Li in the  $\alpha$  structure. With a higher Li concentration, stronger structural distortions occur, resulting in a higher  $E_g$ . The  $\text{Li } 2s$  orbitals contribute to both the VBE and CBE at any concentration due to the stronger structural distortion, but their impact is still minor in magnitude.

Figure 8 displays the band structures of  $\alpha\text{-Li}_x\text{CsPbI}_3$  with Li content  $x=1$  at O and T sites to further analyze the hybridization between Li  $2s$  orbitals and the host-crystal orbitals. The Li contribution to the bands is indicated by blue circles. When the Li atoms are located on O sites, the Li  $2s$  states form a recognizable defect level (the bands with dense blue circles) that is more localized and has no contribution to the band edges. On the T site, the hybridization between Li  $2s$  orbitals and Pb  $6p$  orbitals occurs over a broader energy range.

The strength of the orbital overlap can be estimated based on the distances from Li to I and Pb. The nearest Li-I and Li-Pb distances of Li on T sites are 2.53–2.61 Å and 2.70–2.97 Å, respectively. For Li on O sites, the Li-I and Li-Pb distances are larger, 2.88–3.09 Å and 4.36–4.39 Å, respectively. As a result, the increased overlap estimated from the smaller spatial distance in case of the T site is consistent with a broadened Li  $2s$  contribution that extends closer to the band edges for Li on T sites. However, in either case, the Li  $2s$  contribution to the band edges is negligible compared to the manifold of I and Pb states, cf. Fig. 7a.

So far, we have analyzed the case of inserting neutral Li atoms into the neutral perovskite crystal. Besides the  $2s$  orbital, which appears to have a weak effect on the band edges, the insertion of a Li atom also introduces an additional electron into the  $\text{CsPbI}_3$  crystal. In this scenario, the Fermi level ( $E_F$ ) shifts into the conduction band, and the band gap of  $\text{CsPbI}_3$  with Li in the O sites changes by 0.21 eV from  $x=0$  to  $x=1$ , even without any structural alterations. This indicates that the extra electron in the conduction band directly influences the electronic structure. We quantify this effect in three different  $\alpha$  structures, the one for  $x=0$  as well as the cases  $x=1$  with Li in O and T sites, respectively. Here, we

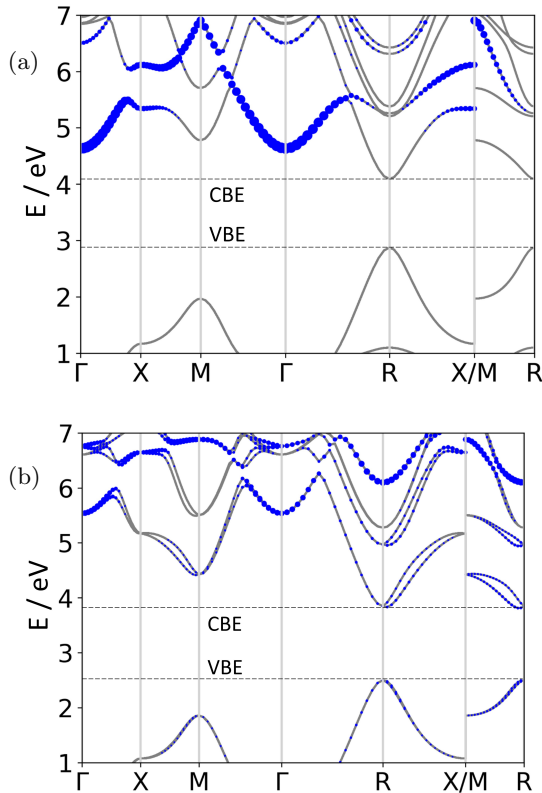


FIG. 8: Band structure of  $\text{Li}_x\text{CsPbI}_3$  with Li atoms on the a) O and b) T sites for  $x = 1$  in the  $\alpha$  structure. Li contributions to bands are indicated by blue circles. The circle radius indicates the magnitude of the contribution.

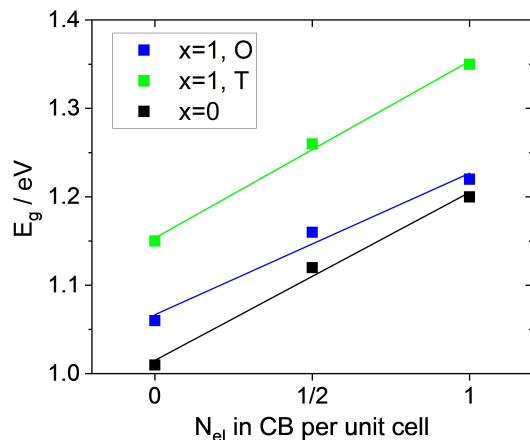


FIG. 9: Band gap change with varying number of electrons in the conduction band for three  $\alpha$  structures of  $\text{Li}_x\text{CsPbI}_3$  with  $x = 0$  and  $x = 1$  with Li atoms at O or T sites.

keep the crystal structures unchanged when varying  $N_{\text{el}}$ .

The relationship between  $E_g$  and the number of excess electrons per perovskite formula unit,  $N_{\text{el}}$ , is illustrated in Fig. 9. In all three investigated cases, the band gap increases with  $N_{\text{el}}$ ; this behavior is rather well described by a linear relation. The three slopes vary only between 0.16 and 0.20 eV per electron. This means that the influence of extra electrons at the CBE in  $\text{Li}_x\text{CsPbI}_3$  alloys on the band gap can be modeled by an average shift of approximately 0.18 eV per extra electron.

We can use this relationship to subtract the influence of the extra charges by subtracting  $x \cdot 0.18$  eV from the computed band gap values. Doing so, our computed structures serve as representative model structures for dilute  $\text{Li}_x\text{CsPbI}_3$  alloys with very small  $x$ , where the structural changes of Li dopants occur locally, but the extra electrons may be delocalized. This description of this dilute limit is, however, not our main focus, having a battery application and, thus, large  $x$  in mind.

In the concentration range of interest, we can use the above relation to isolate the structural influence on the band gap from the two influences of Li (extra electrons and band hybridization) that also contribute to the relation between  $E_g$  and  $\Delta_{\text{Pb-I-Pb}}$ .

The resulting behavior without the additional influence of extra electrons is displayed in Fig. 6 (b). As noted above, the region of  $\gamma'$ -like structures is well represented by a linear relationship. Likewise, the structures with Li being added to the  $\alpha$  structure are described well by a linear relationship. Accounting for the influence of a varying amount of extra electrons the outlier mentioned above for Li on the O site with  $x=1$  fits well now to the linear relation.

However, slope and axis intercept of the two linear regimes differ. The first reason for this difference is the different volume when comparing the  $\alpha$ -like and  $\gamma'$ -like (or  $\gamma$ -phase) structures. For comparison we show the data (blue points in Fig. 6 (b)) for the high-symmetry cases for the  $\alpha$  structures with the larger volume that is calculated using the PBE functional (without the TS correction, see computational details). The resulting slope, compared to the results in the smaller volume (of PBE with TS), is almost unchanged, although the two lines differ in their y-axis intercepts. By scaling the averaged relationship between  $E_g$  and  $\Delta_{\text{Pb-I-Pb}}$  of the data sets to both volumes, we derive the relationship for the volume of the  $\gamma'$  structure (magenta line). This intercepts the linear relationship of  $\gamma'$  type structures for  $x=0$ , i.e., we obtain a continuous transition from  $\alpha$ -like to  $\gamma'$ -like structures when increasing  $\Delta_{\text{Pb-I-Pb}}$ . The remaining different slope is attributed to the fact that Li ions in the  $\alpha$  structure affect the Pb-I-Pb bond angles very locally, as long as (some) symmetry elements of the  $\alpha$  phase are retained. In these cases, the obtained band gap is affected by bands from both tilted and untilted Pb-I-Pb angles. This is distinct from the  $\gamma'$  type structures, where all Pb-I-Pb angles are already tilted. Hence, a change in slope between the two linear regimes is plausible.

We also analyzed a removal of all Li contributions, i.e., we determined the CsPbI<sub>3</sub> structures with the distortions caused by Li atoms, and then we removed the Li atoms when evaluating the electronic structure (i.e., the extra electrons, the 2s bands, and the ionic cores of Li are omitted). We find that the influence on  $E_g$ , coming only from the structural changes of the CsPbI<sub>3</sub> lattice in that way does only in some cases correlate well with the band-gap data given in Fig. 6 (b). In about half of the cases, the interactions that are omitted when removing Li as bonding partner lead to significant changes in the local DOS of the Iodine  $p$  orbitals that are directed towards Li. Thus, the change of  $E_g$  with the Li content is dominated by the structural changes of the CsPbI<sub>3</sub> lattice (see Fig. 6 (a)), and one can describe these changes by separating the structural effect from the varying amount of extra electrons in the conduction band (Fig. 6 (b)). But describing the observed band-gap variation purely by the structural changes of the CsPbI<sub>3</sub> lattice and neglecting the presence of Li as bonding partner is not successful.

#### IV. DISCUSSION

The ordered cubic  $\alpha$  structure has served as the structural model of choice in most previous theoretical studies [16, 17, 37]. However, recent studies [31–33, 38] suggest that this model is probably not the preferred structural representation of the dynamic CsPbI<sub>3</sub> crystal around room temperature and the  $\gamma'$  structure is a more reasonable model. We find that the latter choice is even more relevant when adding Li to the structure, which itself promotes the occurrence of octahedral tilts in our results, cf. Fig. 3.

According to our simulation results, the limit for Li uptake into a hypothetical high symmetry  $\alpha$  structure would be  $x=1/4$ , cf. Fig. 2. This is in line with the DFT results of Dawson et al. (from  $x=0.037$  to  $x=1$ ) on MAPbI<sub>3</sub> and MAPbBr<sub>3</sub> [10]. These results indicate that both hybrid halide perovskites cannot bear a Li concentration of  $x=1$ , and perovskite dissolution or distortion is energetically preferred. Similarly, Büttner et al. [7] reported that the electrolytes containing Li dissolve the perovskite immediately, and they concluded the impossibility to store Li ions in the hybrid halide perovskites. This can be explained with the ability of the organic cations in hybrid perovskites to form hydrogen bonds to polar solvent molecules, which facilitates the perovskite decomposition [39]. This decomposition is even thermodynamically favorable for Pb-based hybrid halide perovskites [40]. In contrast, the inorganic CsPbI<sub>3</sub> perovskites are thermodynamically stable [40].

As opposed to the case of the  $\alpha$  structure, the formation energy of interstitial Li in the  $\gamma'$  structure increases with increasing  $\Delta_{\text{Pb-I-Pb}}$  for the most stable O and T sites at low Li concentration, cf. Fig. 4. Thereafter, for  $x=1/2$ , the formation energy reaches a plateau, while the structural distortion still increases with increasing con-

centration. Overall, the energy profile is in line with a stabilization of the  $\gamma'$  structure, with the lowest energy obtained for the Li-containing structure that is closest to the  $\gamma'$  structure. The formation energies in a range from -0.26 eV to -0.11 eV (from  $x=1/8$  to 1) indicate the potential for battery applications.

Higher Li concentrations with  $x > 1$  distort the perovskite structure, altering the cubic lattice by the displacement of Pb ( $\Delta_{\text{dPb}}$ ) instead of only changing the Pb-I-Pb angles ( $\Delta_{\text{Pb-I-Pb}}$ ), cf. Fig 5. This structural distortion differs significantly from the conditions of Li in the  $\alpha$  structure and the lower Li concentrations in the  $\gamma'$  structure. We propose that it is unfeasible to maintain the perovskite structure in high concentrations of Li, whereby the limiting concentration of Li is  $x=1$ .

Interestingly, as the concentration of Li increases beyond  $x=1$ , the structural change is accompanied by a lower formation energy than for  $x < 1$ . It indicates a high capacity of the material for Li storage. Similar results have been reported from experiments [8, 9]. Xia et al. demonstrated an astonishingly high Li concentration with  $x \approx 6$  in Li<sub>*x*</sub>MAPbBr<sub>3</sub>, although the Li capacity faded rapidly after only 30 charge/discharge cycles. Vicente et al. reported that the Li concentration in Li<sub>*x*</sub>MAPbBr<sub>3</sub> reaches a value as high as  $x = 3.7$ . The rapid fading of the high Li capacity indicates structural distortion away from the perovskite structure, which is in line with our results for high Li concentrations.

Finally, we found that the insertion of Li increases the band gap of the CsPbI<sub>3</sub> perovskite, cf. Fig 6. Similar results for Li containing perovskite compounds were reported from photoluminescence experiments [13, 14, 41]. Jiang et al. [13] found a blue shift in the photoluminescence spectrum by Li inserted in CsPbBr<sub>3</sub>, and attributed it to the Burstein–Moss effect [42]. This effect refers to the phenomenon that electrons at the VBE require higher energies to be excited due to the occupation of the CBE, thus exhibiting a higher absorption band gap. A similar blue shift was also found in Li<sub>*x*</sub>MAPbBr<sub>3</sub> by Mathieson et al. [14]. They suggested that although the inserted Li atoms narrow the band gap, the electrons can only be excited by photons of higher energy due to the occupied CBE. However, the influence of the Li atoms on the band gap of the perovskite crystal is multifaceted, and the mechanism mentioned in the cited literature is only about the occupied CBE. According to our results, the main reason for the increased band gap is the inevitable structural distortion induced by the Li atoms.

The band gap increase caused by the inserted Li is determined by the covalent bonding character of the halide perovskite. The VBE and CBE of CsPbI<sub>3</sub> are mainly composed of the covalent  $\sigma^*$ -bonding states of  $p$  and  $s$  orbitals of Pb and I [43], and the dispersion of the bands is determined by the overlaps of these orbitals. The insertion of Li atoms increases the  $\Delta_{\text{Pb-I-Pb}}$  by attracting I atoms and, thus, reducing the overlap between the Pb and I orbitals. As a result, the presence of Li

significantly increases the band gap, finally rendering three-dimensional halide-perovskite crystals not suitable for the use in photo-battery devices. But the organic-inorganic hybrid layers in two-dimensional perovskites may be more promising for Li storage and photovoltaic function. Ahmad et al. demonstrated the insertion of Li ions into a perovskite compound with a capacity of approx. 100 mAh/g and without compromising the photovoltaic efficiency [44]. Li is stored in the organic layer of the two-dimensional perovskite, which does not affect the band gap of the inorganic perovskite layer. Furthermore, Chen et al. [45] proposed a plausible Li storage mechanism involving carbonyl groups. The aforementioned mechanism (or related ones) holds the potential for developing an integrated halide-perovskite photo-battery.

## V. SUMMARY

In this work, the stability of Li intercalated into CsPbI<sub>3</sub> is analyzed together with the effect that Li has on the electronic structure of the resulting Li<sub>x</sub>CsPbI<sub>3</sub> compounds. We analyze this by two structural models for CsPbI<sub>3</sub>: first, the cubic perovskite  $\alpha$  structure, which is a hypothetical structure to be understood as a reference model with negligible probability to occur at room temperature; second, a distorted  $\gamma'$  structure, closely related to the  $\gamma$  phase, that represents the lowest energy structure at room temperature. The hypothetical  $\alpha$  structure energetically disfavors Li uptake and is likely to be structurally unstable for  $x > 1/4$ . Thus, such a theoretical model is unsuitable for interpreting experiments that demonstrate the existence of Li<sub>x</sub>CsPbI<sub>3</sub> compounds.

In the  $\gamma'$  structure, interstitial insertion of Li is energetically favorable. Concentrations up to  $x = 1$  are accessible while keeping the perovskite host structure intact. In principle, forming the compound with even higher Li

concentration is feasible. However, our investigation of structures with up to  $x = 2$  indicate that in such cases significant distortions of the host lattice structure occur. The structural distortions of such phase transitions and their potential irreversibility require further investigations.

For the concentration range  $0 \leq x \leq 1$ , Li promotes structural distortions, namely increased Pb-I-Pb bond angles and Cs off-center displacements, which increase with the Li concentration. Interstitial Li has several effects on the electronic structure of Li<sub>x</sub>CsPbI<sub>3</sub>: i) the induced structural distortion reduces the band dispersion, leading to a significant increase of the band gap; ii) the electronic screening of extra electrons in the conduction band leads to a slight increase of the band gap; iii) although the Li 2s orbitals hybridize with I and Pb orbitals, their effect on the band gap and the band edges is negligible. Nevertheless, the (presumably fairly ionic) bonding interaction of the Li cation with the surrounding iodine anions does modulate the observed band gap.

Altogether, these effects result in an increased band gap in Li<sub>x</sub>CsPbI<sub>3</sub> compared to CsPbI<sub>3</sub>. The band gap  $E_g$  increases linearly with the induced averaged angle distortion  $\Delta_{\text{Pb-I-Pb}}$  in the two structural regimes of the  $\alpha$  and  $\gamma'$  models. For  $x=1$ , this leads to  $E_g$  of 2.99 eV. This continuously increasing band gap needs to be taken into account for potential solar cell applications.

## ACKNOWLEDGMENTS

This work was supported by the Deutsche Forschungsgemeinschaft (DFG, German Research Foundation) under Germany's Excellence Strategy-EXC-2193/1-390951807 (LivMatS). We thank the State of Baden-Württemberg (Germany) through bwHPC for computational resources.

- 
- [1] C. S. Lai, Y. Jia, L. L. Lai, Z. Xu, M. D. McCulloch, and K. P. Wong, A comprehensive review on large-scale photovoltaic system with applications of electrical energy storage, *Renewable and Sustainable Energy Reviews* **78**, 439 (2017).
  - [2] Y. Arora, C. Seth, and D. Khushalani, Crafting inorganic materials for use in energy capture and storage, *Langmuir* **35**, 9101 (2018).
  - [3] T. Berestok, C. Diestel, N. Ortlieb, S. W. Glunz, and A. Fischer, A monolithic silicon-mesoporous carbon photosupercapacitor with high overall photoconversion efficiency, *Advanced Materials Technologies* **7**, 2200237 (2022).
  - [4] L. Zhang, J. Miao, J. Li, and Q. Li, Halide perovskite materials for energy storage applications, *Advanced Functional Materials* **30**, 2003653 (2020).
  - [5] Z. Li, C. Xiao, Y. Yang, S. P. Harvey, D. H. Kim, J. A. Christians, M. Yang, P. Schulz, S. U. Nanayakkara, C.-S. Jiang, *et al.*, Extrinsic ion migration in perovskite solar cells, *Energy & Environmental Science* **10**, 1234 (2017).
  - [6] J. Zhang, R. Chen, Y. Wu, M. Shang, Z. Zeng, Y. Zhang, Y. Zhu, and L. Han, Extrinsic movable ions in MAPbI<sub>3</sub> modulate energy band alignment in perovskite solar cells, *Advanced Energy Materials* **8**, 1701981 (2018).
  - [7] J. Büttner, T. Berestok, S. Burger, M. Schmitt, M. Daub, H. Hillebrecht, I. Krossing, and A. Fischer, Are halide-perovskites suitable materials for battery and solar-battery applications—fundamental reconsiderations on solubility, lithium intercalation, and photo-corrosion, *Advanced Functional Materials* **32**, 2206958 (2022).
  - [8] H.-R. Xia, W.-T. Sun, and L.-M. Peng, Hydrothermal synthesis of organometal halide perovskites for Li-ion batteries, *Chemical Communications* **51**, 13787 (2015).
  - [9] N. Vicente and G. Garcia-Belmonte, Methylammonium lead bromide perovskite battery anodes reversibly host high Li-ion concentrations, *The Journal of Physical Chemistry Letters* **8**, 1371 (2017).
  - [10] J. A. Dawson, A. J. Naylor, C. Eames, M. Roberts,

- W. Zhang, H. J. Snaith, P. G. Bruce, and M. S. Islam, Mechanisms of lithium intercalation and conversion processes in organic–inorganic halide perovskites, *ACS Energy Letters* **2**, 1818 (2017).
- [11] A. Willoughby, Atomic diffusion in semiconductors, *Reports on Progress in Physics* **41**, 1665 (1978).
- [12] C. H. Henry, Limiting efficiencies of ideal single and multiple energy gap terrestrial solar cells, *Journal of Applied Physics* **51**, 4494 (1980).
- [13] Q. Jiang, X. Zeng, N. Wang, Z. Xiao, Z. Guo, and J. Lu, Electrochemical lithium doping induced property changes in halide perovskite CsPbBr<sub>3</sub> crystal, *ACS Energy Letters* **3**, 264 (2017).
- [14] A. Mathieson, S. Feldmann, and M. De Volder, Solid-state lithium-ion batteries as a method for doping halide perovskites with an in situ optical readout of dopant concentration, *JACS Au* **2**, 1313 (2022).
- [15] S. Mahato, A. Ghorai, S. K. Srivastava, M. Modak, S. Singh, and S. K. Ray, Highly air-stable single-crystalline  $\beta$ -CsPbI<sub>3</sub> nanorods: A platform for inverted perovskite solar cells, *Advanced Energy Materials* **10**, 2001305 (2020).
- [16] J. Zhang, L. Yang, Y. Zhong, H. Hao, M. Yang, and R. Liu, Improved phase stability of the CsPbI<sub>3</sub> perovskite via organic cation doping, *Physical Chemistry Chemical Physics* **21**, 11175 (2019).
- [17] Y.-H. Kye, C.-J. Yu, U.-G. Jong, K.-C. Ri, J.-S. Kim, S.-H. Choe, S.-N. Hong, S. Li, J. N. Wilson, and A. Walsh, Vacancy-driven stabilization of the cubic perovskite polymorph of CsPbI<sub>3</sub>, *The Journal of Physical Chemistry C* **123**, 9735 (2019).
- [18] J. B. Hoffman, A. L. Schleper, and P. V. Kamat, Transformation of sintered CsPbBr<sub>3</sub> nanocrystals to cubic CsPbI<sub>3</sub> and gradient CsPbBr<sub>x</sub>I<sub>3-x</sub> through halide exchange, *Journal of the American Chemical Society* **138**, 8603 (2016).
- [19] R. J. Sutton, M. R. Filip, A. A. Haghighirad, N. Sakai, B. Wenger, F. Giustino, and H. J. Snaith, Cubic or orthorhombic? Revealing the crystal structure of metastable black-phase CsPbI<sub>3</sub> by theory and experiment, *ACS Energy Letters* **3**, 1787 (2018).
- [20] B. Wang, N. Novendra, and A. Navrotsky, Energetics, structures, and phase transitions of cubic and orthorhombic cesium lead iodide (CsPbI<sub>3</sub>) polymorphs, *Journal of the American Chemical Society* **141**, 14501 (2019).
- [21] W. Wei, J. Gebhardt, D. F. Urban, and C. Elsässer, Location and migration of interstitial Li ions in CsPbI<sub>3</sub> crystals, *Physical Review B*, accepted manuscript BH14763 (2024).
- [22] G. Kresse and J. Furthmüller, Efficiency of ab-initio total energy calculations for metals and semiconductors using a plane-wave basis set, *Computational Materials Science* **6**, 15 (1996).
- [23] P. E. Blöchl, Projector augmented-wave method, *Physical Review B* **50**, 17953 (1994).
- [24] J. P. Perdew, K. Burke, and M. Ernzerhof, Generalized gradient approximation made simple, *Physical Review Letters* **77**, 3865 (1996).
- [25] H. J. Monkhorst and J. D. Pack, Special points for brillouin-zone integrations, *Physical Review B* **13**, 5188 (1976).
- [26] T. Bučko, J. Hafner, and J. G. Ángyán, Geometry optimization of periodic systems using internal coordinates, *The Journal of Chemical Physics* **122**, 124508 (2005).
- [27] A. Tkatchenko and M. Scheffler, Accurate molecular van der waals interactions from ground-state electron density and free-atom reference data, *Physical Review Letters* **102**, 073005 (2009).
- [28] G. E. Eperon, G. M. Paternò, R. J. Sutton, A. Zampetti, A. A. Haghighirad, F. Cacialli, and H. J. Snaith, Inorganic caesium lead iodide perovskite solar cells, *Journal of Materials Chemistry A* **3**, 19688 (2015).
- [29] L. G. Ferreira, M. Marques, and L. K. Teles, Approximation to density functional theory for the calculation of band gaps of semiconductors, *Physical Review B* **78**, 125116 (2008).
- [30] S. Steiner, S. Khmelevskiy, M. Marsmann, and G. Kresse, Calculation of the magnetic anisotropy with projected-augmented-wave methodology and the case study of disordered Fe<sub>1-x</sub>Co<sub>x</sub> alloys, *Physical Review B* **93**, 224425 (2016).
- [31] J. Gebhardt, W. Wei, and C. Elsässer, Efficient modeling workflow for accurate electronic structures of hybrid perovskites, *The Journal of Physical Chemistry C* **125**, 18597 (2021).
- [32] P. Whitfield, N. Herron, W. Guise, K. Page, Y. Cheng, I. Milas, and M. Crawford, Structures, phase transitions and tricritical behavior of the hybrid perovskite methyl ammonium lead iodide, *Scientific Reports* **6**, 1 (2016).
- [33] R. X. Yang, J. M. Skelton, E. L. Da Silva, J. M. Frost, and A. Walsh, Spontaneous octahedral tilting in the cubic inorganic cesium halide perovskites CsSnX<sub>3</sub> and CsPbX<sub>3</sub> (X= F, Cl, Br, I), *The Journal of Physical Chemistry Letters* **8**, 4720 (2017).
- [34] J. Klarbring, Low-energy paths for octahedral tilting in inorganic halide perovskites, *Physical Review B* **99**, 104105 (2019).
- [35] A. Marrognier, G. Roma, S. Boyer-Richard, L. Pedesseau, J.-M. Jancu, Y. Bonnassieux, C. Katan, C. C. Stoumpos, M. G. Kanatzidis, and J. Even, Anharmonicity and disorder in the black phases of cesium lead iodide used for stable inorganic perovskite solar cells, *ACS Nano* **12**, 3477 (2018).
- [36] J. L. Knutson, J. D. Martin, and D. B. Mitzi, Tuning the band gap in hybrid tin iodide perovskite semiconductors using structural templating, *Inorganic Chemistry* **44**, 4699 (2005).
- [37] U.-G. Jong, C.-J. Yu, Y.-S. Kim, Y.-H. Kye, and C.-H. Kim, First-principles study on the material properties of the inorganic perovskite Rb<sub>1-x</sub>Cs<sub>x</sub>PbI<sub>3</sub> for solar cell applications, *Physical Review B* **98**, 125116 (2018).
- [38] J. Wiktor, U. Rothlisberger, and A. Pasquarello, Predictive determination of band gaps of inorganic halide perovskites, *The Journal of Physical Chemistry Letters* **8**, 5507 (2017).
- [39] C. Zheng and O. Rubel, Unraveling the water degradation mechanism of CH<sub>3</sub>NH<sub>3</sub>PbI<sub>3</sub>, *The Journal of Physical Chemistry C* **123**, 19385 (2019).
- [40] Y. Zhou and Y. Zhao, Chemical stability and instability of inorganic halide perovskites, *Energy & Environmental Science* **12**, 1495 (2019).
- [41] H. Wu, J. Qiu, J. Wang, Y. Wen, Q. Wang, Z. Long, D. Zhou, Y. Yang, and D. Wang, The dual-defect passivation role of lithium bromide doping in reducing the nonradiative loss in CsPbX<sub>3</sub> (X= Br and I) quantum dots, *Inorganic Chemistry Frontiers* **8**, 658 (2021).
- [42] E. Burstein, Anomalous optical absorption limit in InSb,

- Physical Review **93**, 632 (1954).
- [43] T. Umebayashi, K. Asai, T. Kondo, and A. Nakao, Electronic structures of lead iodide based low-dimensional crystals, *Physical Review B* **67**, 155405 (2003).
- [44] S. Ahmad, C. George, D. J. Beesley, J. J. Baumberg, and M. De Volder, Photo-rechargeable organo-halide perovskite batteries, *Nano Letters* **18**, 1856 (2018).
- [45] Y. Chen, Z. Chen, X. Zhang, J. Chen, and Y. Wang, An organic-halide perovskite-based photo-assisted Li-ion battery for photoelectrochemical storage, *Nanoscale* **14**, 10903 (2022).
- [46] H. Beck, C. Gehrman, and D. A. Egger, Structure and binding in halide perovskites: analysis of static and dynamic effects from dispersion-corrected density functional theory, *APL Materials* **7**, 021108 (2019).
- [47] M. Kim, W. J. Kim, T. Gould, E. K. Lee, S. Lebègue, and H. Kim, umbd: A materials-ready dispersion correction that uniformly treats metallic, ionic, and van der waals bonding, *Journal of the American Chemical Society* **142**, 2346 (2020).
- [48] M. Kepenekian, R. Robles, C. Katan, D. Saponi, L. Pedesseau, and J. Even, Rashba and Dresselhaus effects in hybrid organic-inorganic perovskites: from basics to devices, *ACS Nano* **9**, 11557 (2015).
- [49] L. D. Whalley, J. M. Frost, Y.-K. Jung, and A. Walsh, Perspective: Theory and simulation of hybrid halide perovskites, *The Journal of Chemical Physics* **146**, 220901 (2017).
- [50] P. Mori-Sánchez, A. J. Cohen, and W. Yang, Localization and delocalization errors in density functional theory and implications for band-gap prediction, *Physical Review Letters* **100**, 146401 (2008).
- [51] J. P. Perdew and M. Levy, Physical content of the exact kohn-sham orbital energies: band gaps and derivative discontinuities, *Physical Review Letters* **51**, 1884 (1983).
- [52] L. J. Sham and M. Schlüter, Density-functional theory of the energy gap, *Physical Review Letters* **51**, 1888 (1983).
- [53] S. X. Tao, X. Cao, and P. A. Bobbert, Accurate and efficient band gap predictions of metal halide perovskites using the DFT-1/2 method: GW accuracy with DFT expense, *Scientific Reports* **7**, 1 (2017).
- [54] R. E. Brandt, J. R. Poindexter, P. Gorai, R. C. Kurchin, R. L. Hoyer, L. Nienhaus, M. W. Wilson, J. A. Polizzotti, R. Sereika, R. Zaltauskas, *et al.*, Searching for "defect-tolerant" photovoltaic materials: combined theoretical and experimental screening, *Chemistry of Materials* **29**, 4667 (2017).
- [55] G. Makov and M. Payne, Periodic boundary conditions in ab initio calculations, *Physical Review B* **51**, 4014 (1995).
- [56] J. Neugebauer and M. Scheffler, Adsorbate-substrate and adsorbate-adsorbate interactions of Na and K adlayers on Al (111), *Physical Review B* **46**, 16067 (1992).
- [57] B. Luo, D. Ye, and L. Wang, Recent progress on integrated energy conversion and storage systems, *Advanced Science* **4**, 1700104 (2017).
- [58] P. Umari, E. Mosconi, and F. De Angelis, Relativistic GW calculations on  $\text{CH}_3\text{NH}_3\text{PbI}_3$  and  $\text{CH}_3\text{NH}_3\text{SnI}_3$  perovskites for solar cell applications, *Scientific Reports* **4**, 1 (2014).
- [59] A. Kojima, K. Teshima, Y. Shirai, and T. Miyasaka, Organometal halide perovskites as visible-light sensitizers for photovoltaic cells, *Journal of the American Chemical Society* **131**, 6050 (2009).